

# A novel metal–organic coordination polymer for selective adsorption of CO<sub>2</sub> over CH<sub>4</sub>†

Bin Mu, Feng Li and Krista S. Walton\*

Received (in Cambridge, UK) 6th November 2008, Accepted 25th February 2009

First published as an Advance Article on the web 30th March 2009

DOI: 10.1039/b819828d

**A unique two-dimensional interpenetrating network structure possessing unsaturated metal sites and uncoordinated carboxylic functional groups exhibits among the highest reported adsorption selectivities for CO<sub>2</sub> over CH<sub>4</sub>.**

Porous coordination polymers or metal–organic frameworks (MOFs) have attracted great interest recently for potential applications in adsorption separations, gas storage, sensing, and catalysis.<sup>1</sup> In contrast to conventional microporous materials, these organic–inorganic hybrids have the potential for synthesis using a rational design approach by flexible control of the architecture and functional group.<sup>2</sup> In materials such as those assembled from the paddle-wheel structure, as-synthesized MOFs have solvent molecules attached as ligands to the metal centers. Removal of these solvent ligands by thermal activation generates unsaturated metal centers (UMCs) or open metal sites. Thus, the metal atoms are exposed on the interior surfaces of the material and are open to direct approach by sorbate molecules. These exposed metal sites can be seen as analogous to entatic metal centers in bioinorganic chemistry, in which metal ions are forced into unusual coordination geometry like the iron in hemoglobin.<sup>3</sup> Open metal sites greatly increase the ability of the material to selectively adsorb particular molecules. Consequently, the incorporation of UMCs into MOFs is a practical strategy for manipulating the adsorption behavior.

There have been a number of reports in recent years of MOFs with UMCs.<sup>1c,4</sup> Many of these materials possess 3D structures with channels or interconnected pores. The adsorption properties of a particular material will depend on this structure dimensionality in combination with porosity and pore size, surface area, and presence or absence of open metal sites. Thus, it is necessary to understand the complex interplay of these factors in affecting adsorption behavior to move towards a rational design of these materials for adsorption applications.

In this work, we report a unique interpenetrating two-dimensional network structure with uncoordinated carboxylic functional groups and unsaturated Cu<sup>2+</sup> ions which display a

Jahn–Teller distortion. Green diamond-shaped crystals of [Cu<sub>2</sub>(HBTB)<sub>2</sub>(H<sub>2</sub>O)(EtOH)]·H<sub>2</sub>O·EtOH (**1**) were harvested from the reaction of H<sub>3</sub>BTB (H<sub>3</sub>BTB = 1,3,5-tris(4-carboxyphenyl) benzene) with Cu(NO<sub>3</sub>)<sub>2</sub>·3H<sub>2</sub>O in a mixture of ethanol and water at 110 °C. This material assembles in 2D sheets that are stacked through hydrogen bonding. Channels resembling coils are formed by the helical chains. The composition of **1** was confirmed by single-crystal X-ray diffraction, and the phase purity of the bulk sample was confirmed by powder XRD. TGA analysis shows that the compound **1** is stable up to 300 °C. The BET surface area was calculated<sup>5</sup> from nitrogen adsorption at 77 K to be approximately 600 m<sup>2</sup> g<sup>-1</sup>.

X-Ray diffraction analysis reveals that **1** is a 2-fold parallel interpenetrating (4,4) 2D network.† As shown in Fig. 1, four crystallographically independent copper atoms are present, which are all five-coordinated in square pyramid coordination geometry. Cu1(Cu2) is coordinated by one water molecule and four oxygen atoms from four carboxyl groups. Cu3(Cu4) is coordinated by one ethanol molecule and four oxygen atoms from four carboxyl groups. Four carboxyl groups link Cu1 and Cu2 (Cu3 and Cu4) into the paddle-wheel cluster motif with a Cu1–Cu2 distance of 2.589(4) Å (Cu3–Cu4 2.618(4) Å).

Due to the different coordination environment between Cu1(Cu2) and Cu3(Cu4), the respective paddle-wheel units also display some differences (Fig. 1). In **1**, the H<sub>3</sub>BTB ligands are partially deprotonated. Two carboxyl groups of this ligand are deprotonated and coordinated to the copper ions with bidentate coordination mode. The third carboxyl group is protonated and does not take part in the coordination. Thus, each HBTB<sup>2-</sup> connects two adjacent Cu1–Cu2 and Cu3–Cu4 paddle-wheel clusters into 2<sub>1</sub> helical chains along the *b* axis. Each unit of the helical chain contains one Cu1–Cu2 and one Cu3–Cu4 paddle-wheel cluster (the helical pitch, given by one full rotation around the 2<sub>1</sub> helical axis, is 12.56 Å). As

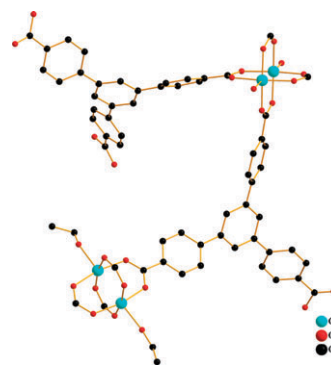


**Fig. 1** View of the coordination about the Cu atoms. (All solvent molecules and hydrogen atoms are omitted for clarity.)

Department of Chemical Engineering, Kansas State University,  
1005 Durland Hall, Manhattan, KS 66506, USA.

E-mail: k Walton@ksu.edu; Fax: +1-785-532-7372;

Tel: +1-785-532-4316

† Electronic supplementary information (ESI) available: Materials synthesis and activation details, crystallographic information, powder-XRD pattern, nitrogen adsorption isotherm, TGA curves, elemental analysis, and FTIR pattern of crystal **1**. CCDC 708312. For ESI and crystallographic data in CIF or other electronic format see DOI: 10.1039/b819828d

mentioned above, four carboxyl groups link two copper atoms into one paddle-wheel cluster. Two of the four carboxyl groups of each paddle-wheel cluster link Cu1–Cu2 and Cu3–Cu4 clusters into one left-handed helical chain, and the other two carboxyl groups of each cluster compose one unit of a right-handed helical chain. In compound **1**, left- and right-handed helical chains coexist and array alternately. Through sharing Cu–Cu paddle-wheel clusters, adjacent helical chains are linked into (4,4) 2D layers at the [100] plane (Fig. S2, ESI†). Such change in dimensionality and crystal structure is due to partial deprotonation of the H<sub>3</sub>BTB ligand, which produces significant alterations in functionality compared to another known Cu–BTB crystal, MOF-14.<sup>1e</sup> Yaghi *et al.* synthesized MOF-14 by solvothermal reaction of H<sub>3</sub>BTB and Cu(NO<sub>3</sub>)<sub>2</sub> in a mixture of ethanol, DMF, water and pyridine. In MOF-14, three carboxyl groups of H<sub>3</sub>BTB are all deprotonated and coordinated to copper centers, which results in a 3D interwoven metal–organic framework with extra-large pores. A sphere 16.4 Å in diameter can fit inside each cavity. Due to the absence of DMF and pyridine in this work, H<sub>3</sub>BTB ligands are only partially deprotonated in **1**, which results in a 2D network containing helical chains (Fig. 2). Though the helical channels are smaller than the cavities of MOF-14, the smaller channels may be more suitable for selective adsorption.

When exploring the acting forces that exist between sheets, weak hydrogen bonding interactions were observed between the coordinated water oxygen atoms from one layer and the coordinated carboxyl oxygen atoms from the second neighboring layer (3.091 Å and 3.043 Å). Through hydrogen bonds, two helical chains from two individual nets are linked into a double-stranded helical chain. The weak hydrogen bonds between sheets result in a 2-fold parallel interpenetrating 2D layer (Fig. S3, ESI†). In previous reports of such networks, the individual networks involved in 2D interpenetration are usually based on the (4,4) or (6,3) net with one exception (8<sup>2</sup>·10).<sup>6</sup> However, it is seldom that dinuclear metal species have been introduced into a 2-fold parallel interpenetrating (4,4) net.<sup>7</sup> To make parallel interpenetration possible, the individual 2D networks must be corrugated or possess some appropriate element of undulation.<sup>8</sup> In **1**, each side of the rhombus windows of the 2D net is actually one repeating unit of the helical chain. The undulation and flexibility of the helical chain make one 2D net pass through the other an infinite number of times, which is different from the corrugation of the whole 2D network.

At the [010] plane, like two open arms, the dangling phenyl rings with uncoordinated carboxyl groups protrude perpendicularly from both sides of the sheets. The effective length of

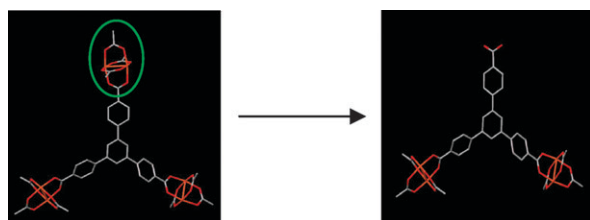


**Fig. 2** 3D to 2D dimensional change coming from partial deprotonation of H<sub>3</sub>BTB ligand.

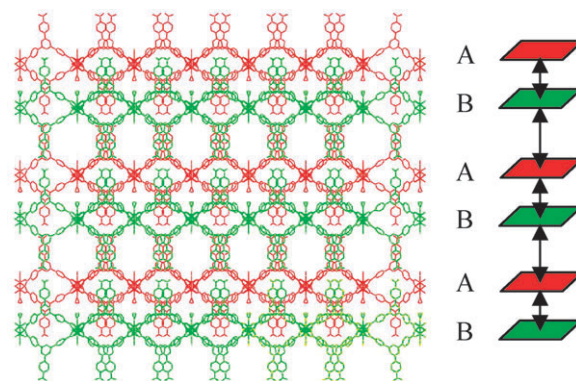


**Fig. 3** The stack of different layers A (red), B (green) at [010] plane (all solvent molecules and hydrogen atoms are omitted for clarity).

each arm is *ca.* 7.18 Å (from the centroid of the central benzyl group to the uncoordinated carboxyl carbon atom). Along the *a* axis, all the layers are stacked on top of each other. However, the layers are not arrayed at the same distance. As shown in Fig. 3, the distance between layer A and layer B (9.601 Å) is short enough that the uncoordinated carboxyl arms of layer A are threaded into the helical channels of layer B in a mutual relationship. The helical channels are then partially occupied by these arms, and the threading results in the formation of bilayers (AB). The arms between two bilayers (AB–AB) are not threaded into each other. The distance between two bilayers (AB–AB) is longer (15.491 Å) than the distance between sheets within a bilayer (A–B).

Upon activation of **1**, the copper atoms become coordinatively unsaturated, which should be expected to enhance the adsorption of dipolar or quadrupolar molecules. Because **1** presents 2D sheets without interconnected pores, this material provides an ideal system for examining the impact of UMCs on adsorption. CO<sub>2</sub>–CH<sub>4</sub>, which is a difficult and important separation in biogas upgrading and natural gas purification, was chosen as a model mixture for examining the separation capability of **1**.

High-pressure single-component adsorption measurements were performed with a gravimetric system. Fig. 4 displays the single-component adsorption isotherms of these gases in **1** at 298 K. CO<sub>2</sub> is more strongly adsorbed than CH<sub>4</sub>, which is expected because CO<sub>2</sub> has a significant quadrupole moment, whereas CH<sub>4</sub> is essentially nonpolar. Neither molecule reaches its saturation loading over the pressure range examined

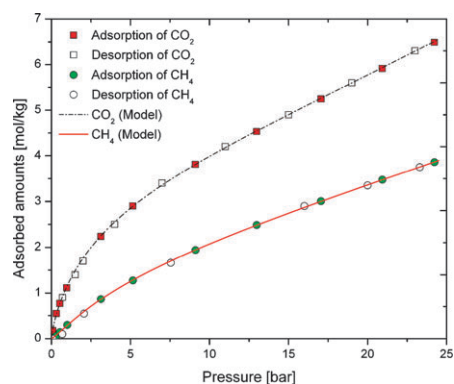


**Fig. 4** Single-component isotherms of CO<sub>2</sub>, CH<sub>4</sub> in **1** at 298 K.

(up to 25 bar). It is shown in Fig. 4 that the adsorption isotherms are reversible, and there is no hysteresis.

Multi-component adsorption equilibrium data are essential for designing adsorption-based separation processes. Components often experience competitive adsorption from mixtures, which results in mixture adsorption isotherms that differ significantly from pure-component behavior. To examine mixture behavior, multi-component isotherms and selectivities for CO<sub>2</sub>–CH<sub>4</sub> mixture adsorption were calculated using the ideal adsorbed solution theory (IAST).<sup>9</sup>

Before using IAST, an accurate isotherm model must be applied to represent single-component adsorption isotherms. Here, the dual-site Langmuir–Freundlich model provided an excellent fit of the adsorption data as shown in Fig. 4. The fitted isotherm parameters were then used to predict the mixture adsorption in **1** using IAST. The predicted adsorption selectivities for equimolar CO<sub>2</sub>–CH<sub>4</sub> mixture in **1** as a function of total bulk pressure are presented in Fig. 5. As shown in the figure, this material displays very high selectivities for CO<sub>2</sub> at low pressure. At 298 K, the calculated selectivity for equimolar CO<sub>2</sub>–CH<sub>4</sub> in activated **1** is near 12.4 at 1 bar. This is much higher than the reported values in Cu-BTC and MOF-5 which displayed selectivities of 6 and 2, respectively, independent of gas-phase composition under the same conditions by GCMC simulation.<sup>10a</sup> The selectivities here are also higher than the values in MFI zeolite and nanoporous carbon membranes, which were reported as 2.5 and 5.2, respectively.<sup>10b</sup> The selectivity decreases with increasing bulk pressure as copper sites become inaccessible. However, even at a total pressure of 20 bar, the selectivity is still close to 5.

Comparing IAST selectivities with those calculated from the pure-component isotherms (Fig. 5), we find that **1** adsorbs CO<sub>2</sub> preferentially from the mixture with methane. Thus, methane adsorbs less than its pure-component loadings due to competition with CO<sub>2</sub>. If competitive adsorption did not exist between CO<sub>2</sub> and methane, then the IAST selectivities would match the selectivities calculated from pure-component loadings.

As a contrast, consider the results of Cu-BTC, which possesses UMCs and 3D interconnected pores. In that material we see that methane is quite attracted to the 3D pore

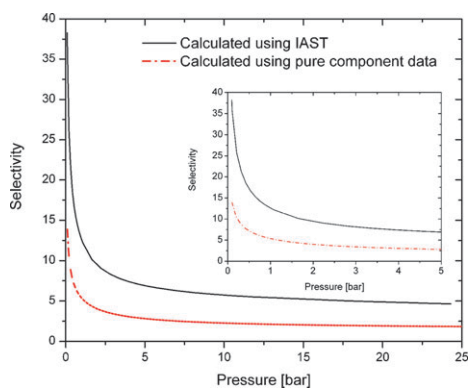


**Fig. 5** Selectivity of CO<sub>2</sub> over CH<sub>4</sub> in **1** for equimolar mixtures of CO<sub>2</sub> and CH<sub>4</sub> at 298 K.

space, which competes with the attraction of CO<sub>2</sub> to UMCs. Thus, selectivities are relatively low (~6). Our material **1** possesses no comparable pores but an abundance of open copper sites. Thus, we have decreased the adsorption potential for methane and increased the selectivity for CO<sub>2</sub> (~13).

In summary, experiments and IAST calculations have shown that activated product **1** is a promising material for the separation and purification of CO<sub>2</sub> from CO<sub>2</sub>–CH<sub>4</sub> mixtures. From a design standpoint, these results imply that constructing MOFs with unsaturated metal centers is of paramount importance for selective adsorption of polar molecules over nonpolar molecules. Furthermore, while somewhat counterintuitive, it appears that for CO<sub>2</sub>–CH<sub>4</sub> and similar mixtures, the presence of 3D interconnected pores can actually be detrimental to adsorption selectivities due to the increase in van der Waals interactions for both polar and nonpolar molecules.

This material is based upon work supported by the Army Research Office under contract W911NF-07-1-0355.

## Notes and references

‡ Crystal data. C<sub>456</sub>H<sub>308</sub>Cu<sub>16</sub>O<sub>142</sub>,  $M = 9075.84$ , orthorhombic,  $a = 28.0524(17)$ ,  $b = 14.8658(9)$ ,  $c = 28.7818(18)$  Å,  $U = 12002.6(13)$  Å<sup>3</sup>,  $T = 100$  K, space group *Pbcm*,  $Z = 1$ , 104053 reflections measured, 12040 unique ( $R_{\text{int}} = 0.0891$ ) which were used in all calculations. The final  $wR(F^2)$  was 0.1536 (all data).

- (a) Y.-S. Bae, K. L. Mulfort, H. Frost, P. Ryan, S. Punnathanam, L. J. Broadbelt, J. T. Hupp and R. Q. Snurr, *Langmuir*, 2008, **24**, 8592–8598; (b) A. R. Millward and O. M. Yaghi, *J. Am. Chem. Soc.*, 2005, **127**, 17998–17999; (c) B. Chen, Y. Yang, F. Zapata, G. Lin, G. Qian and E. B. Lobkovsky, *Adv. Mater.*, 2007, **19**, 1693–1696; (d) R.-Q. Zou, H. Sakurai and Q. Xu, *Angew. Chem., Int. Ed.*, 2006, **45**, 2542–2546; (e) B. Chen, M. Eddaoudi, S. T. Hyde, M. O’Keeffe and O. M. Yaghi, *Science*, 2001, **291**, 1021–1023.
- R.-Q. Zou, L. Jiang, H. Senoh, N. Takeichi and Q. Xu, *Chem. Commun.*, 2005, 3526–3528.
- S. Ma and H.-C. Zhou, *J. Am. Chem. Soc.*, 2006, **128**, 11734–11735.
- (a) B. Chen, N. W. Ockwig, A. R. Millward, D. S. Contreras and O. M. Yaghi, *Angew. Chem., Int. Ed.*, 2005, **117**, 4823–4827; (b) M. Dinca, A. Dailly, Y. Liu, C. M. Brown, D. A. Neumann and J. R. Long, *J. Am. Chem. Soc.*, 2006, **128**, 16876–16883; (c) P. D. C. Dietzel, B. Panella, M. Hirscher, R. Blom and H. Fjellvåg, *Chem. Commun.*, 2006, 959–961; (d) H. R. Moon, N. Kobayashi and M. P. Suh, *Inorg. Chem.*, 2006, **45**, 8672–8676; (e) P. M. Forster, J. Eckert, B. D. Heiken, J. B. Parise, J. W. Yoon, S. H. Jung, J.-S. Chang and A. K. Cheetham, *J. Am. Chem. Soc.*, 2006, **128**, 16846–16850; (f) S. S.-Y. Chui, S. M.-F. Lo, J. P. H. Charmant, A. G. Orpen and I. D. Williams, *Science*, 1999, **283**, 1148–1150; (g) B. Chen, M. Eddaoudi, T. M. Reineke, J. W. Kampf, M. O’Keeffe and O. M. Yaghi, *J. Am. Chem. Soc.*, 2000, **122**, 11559–11560.
- This surface area should be considered with caution because low measurements at low relative pressures could not be obtained. Thus, the BET analysis was performed near the saturation point.
- V. H. Thurn and H. Krebs, *Acta Crystallogr., Sect. B: Struct. Crystallogr. Cryst. Chem.*, 1969, **25**, 125–135.
- C. Qin, X. Wang, L. Carlucci, M. Tong, E. Wang, C. Hu and L. Xu, *Chem. Commun.*, 2004, 1876–1877.
- S. R. Batten and R. Robson, *Angew. Chem., Int. Ed.*, 1998, **37**, 1460–1494.
- A. L. Myers and J. M. Prausnitz, *AIChE J.*, 1965, **11**, 121–127.
- (a) Q. Yang and C. Zhong, *J. Phys. Chem. B*, 2006, **110**, 17776–17783; (b) R. Babarao, Z. Hu and J. Jiang, *Langmuir*, 2007, **23**, 659–666.